scientific reports

Check for updates

OPEN

Numerical analysis of Casson nanofluid three-dimensional flow over a rotating frame exposed to a prescribed heat flux with viscous heating

Wael Al-Kouz✉ & Wahib Owhaib

This study investigates heat transfer characteristics and three-dimensional flow of non-Newtonian Casson nanofluid over a linearly stretching flat surface in the rotating frame of a reference. The current model includes the Buongiorno nanofluid model comprises nanoparticles' haphazard motion and thermo-migration. It also considered mechanisms for viscous heating and constant heat flux at the boundary. The nonlinear partial differential system modeling includes the non-Newtonian Casson fluid model and the boundary layer approximation. The system governing equations were nondimensionalized and numerically solved. A parametric study was conducted to analyze the significance of dimensionless parameters on velocities, the concentration, temperatures, Nusselt number, friction factors, and Sherwood number. The study reveals that the Casson nanoliquid temperature enhanced significantly due to the mechanisms of haphazard motion and thermo-migration. The momentum layer thickness of nano Casson fluid reduced due to the rotation phenomenon while the thermal layer structure amended notably. In the absence of rotation, there is no transverse velocity. The thermal layer structure is enhanced owing to the viscous heating process. The intense haphazard motion and thermo-migration mechanisms lead to maximum heat transfer rate at the plate. In addition, results show that the Coriolis force strength elevation shows similar axial and transverse velocities behavior. In addition, the nanoparticle concentration is observed higher due to the rotation aspect and Casson fluid parameter. Furthermore, the Casson fluid factor decreases with velocities, but the trend is the opposite for the high Casson fluid factor. The thermal and solute layer thickness growth is due to the nanoparticles' thermo-diffusion. In conclusion, the larger rotation factor increases the friction factors. The maximum plate heat transfer rate is when higher Nb and Nt are higher.

Nomenclature

a	Stretching rate
Ca	Dimensionaless Casson fluid factor
C	Nanoparticle concentration
C_w	Plate nanoparticles concentration
C_p	Specific heat (J/kg K)
D_B	Brownian diffusion coefficient
D_T	Thermo-migration diffusion coefficient
Ec	Eckert number
f	Dimensionless axial velocity
g	Dimensionless transverse velocity
k	Thermal conductivity (W/m K)
Le	Lewis number
Nb	Brownian motion parameter

Department of Mechanical and Maintenance Engineering, German Jordanian University, Amman 11180, Jordan. ✉email: wael.alkouz@gju.edu.jo

Nt	Thermophoresis parameter
Nu	Nusselt number
Pr	Prandtl number
q_w	Constant heat flux
Re	Reynolds numbers
Ro	Rotation parameter
Sf	Friction factor
Sh	Sherwood number
T	Temperature (K)
T_w	Fluid temperature (K)
T_∞	Ambient temperature (K)
u, v, w	Velocity component along x, y and z-directions (m/s)

Greek symbols

α	Thermal diffusivity (m^2/s)
ζ	Similarity variable
η	Similarity variable
μ	Dynamic viscosity (kg/m s)
ν	Kinematic viscosity (m^2/s)
θ	Dimensionless temperature
Θ	Dimensionless nanoparticle concentration
ρ	Density (kg/m^3)
ρC_p	Casson fluid heat capacity (J/K)
$(\rho C_p)_{np}$	Nanoparticles heat capacity (J/K)
ω	Rotational velocity (1/s)

Subscripts

l	Liquid
np	Nanoparticles

Nowadays, the flow of non-Newtonian fluids plays a crucial role in several industrial applications such as the polymer industry, 3D printers, the production of plastics, paper manufacturing, etc., and numerous technological processes. The study of dynamics of non-Newtonian material is quite challenging to physicists, engineers, and mathematicians owing to the intricacy of these fluids. Numerous non-Newtonian material models are proposed, as a single constitutive equation does not display all possessions of non-Newtonian materials. The power-law material and two or three-grade fluid models are extensively studied in the literature (Andersson and Dandapat[1]; Hassanien[2]; Sadeghy and Sharifi[3]; Serdar and Salih Dokuz[4]; Sajid et al.[5,6]). The power-law model forecasts shear thickening and shear thinning performance. However, it is insufficient in articulating normal stress performance. A two-grade material model exhibit the normal stress effects. However, it is inadequate to express the performance of shear-thinning/thickening (see for more details Aksoy et al.[7]). The Maxwell model is a rate-type non-Newtonian material model that can envisage stress relaxation, but this model is incapable to study shear-dependent viscosity (see Hayat et al.[8]). The Casson material model is another type of non-Newtonian material model which is capable to predict the yield stress and Casson material is a shear-thinning material (see Fung[9]; Dash et al.[10]). In recent years, the Casson fluid model has been used extensively to study the dynamics of non-Newtonian materials owing to its wide range of industrial applications. Pramanik[11] studied the boundary layer transmission of a non-Newtonian Casson material and heat transfer over an exponentially elongating surface with mass suction or injection. He reported that enlarging values of the Casson material factor suppress the velocity layer thickness. Shaw et al.[12] examined the nonlinear convection transmission of Casson material toward a horizontal flat plate with Newton boundary conditions. They remarked that the friction factor at the plate was enhanced by the Casson material factor and buoyancy ratio factor. The Casson material model was utilized by Tamoor et al.[13] to investigate the heat transfer characteristics along with dissipation, magnetism, and Joule heating over a cylinder. They observed that the curvature factor has an analogous stimulus on the velocity, skin friction, temperature, and Nusselt number. The importance of adjustable viscosity and thermal conductivity is presented by Animasaun[14] in the study of the non-Darcy flow of dissipating Casson material with thermophoresis. Raju and Sandeep[15] considered the time-related three-dimensional dynamics of Casson–Carreau materials past an elongated surface. The influence of porous matrix on the dynamics of Casson material is analyzed by Nadeem et al.[16] by considering three-dimensional flow and magnetism aspects. Shehzad et al.[17] extended the problem of Nadeem et al.[16] by considering the internal heat production mechanism. Analysis of cross-diffusion and Rosseland thermal radiation aspects on the 3D dynamics of Casson material over a heated surface is performed by Zia et al.[18]. They remarked that the velocity layer structures were diminished by the Casson material factor. Prasad et al.[19] investigated the 3-directional dynamics of Casson material over a porous slender flat plate subjected to heat production or captivation. Very recently, Salahuddin et al.[20] examined the Casson material flow subjected to the activation energy, internal energy change, and thermophysical properties.

Recently, a vast number of industries merged nanomaterials with their broad applications for their superior properties and variety of implementation methodologies. Examples of such applications include thermal energy storage systems, electronic cooling, advanced nuclear thermal systems, hybrid-powered machines, solar liquid

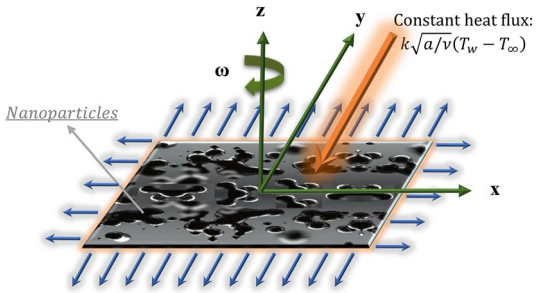

Figure 1. Schematic diagram of the problem under consideration.

heating/cooling, and optoelectronics, etc. Nanofluids are designed by partying tiny solid particles (Al_2O_3, TiO_2, ZnO_2, Cu, Al, Au, etc.) and base fluid (such as ethylene glycol, kerosene, oil, and water). Conveying nanoparticles into the functioning fluids improves the thermal performance of functioning fluids, this fact was first remarked by Choi and Eastman[21]. More industrial applications of using nanofluids are presented Refs.[22–34]. Buongiorno[35] investigated nanoliquids convective heat transfer utilizing a mathematical model that involves two leading mechanisms Brownian motion and thermodiffusion. By utilizing the model proposed by Buongiorno, the boundary layer dynamics of nanofluid toward an upright flat plate were investigated by Kuznetsov and Nield[36]. They reported that the Brownian motion and thermodiffusion mechanisms are accountable for augmenting the temperature boundary layer structure. Minkowycz problem was revisited by Nield and Kuznetsov[37] by employing the Buongiorno model and considering porous matrix effects. Boundary layer transmission of nanomaterial over a horizontal plate is investigated by Khan and Pop[38]. They employed the Keller box method to treat the nonlinear problem and found that the mechanism of the Brownian movement of nanoparticles reduces the concentration of the nanoparticle's layer structure.

The three-directional transmission of magneto-nano Casson material over a plate with Rosseland radiation and Newton boundary condition is investigated by Gupta and Sharma[39]. They utilized the Buongiorno nanofluid model and found that the temperature of Casson fluid enhances by conveying nanoparticles. Nadeem et al.[40] examined the three-dimensional dynamics of magneto-nanofluid over a plate that is elongated with linear velocity. They also scrutinized the influence of the Newton boundary condition. Saeed et al.[41] studied the thin-film dynamics of Casson nanofluid past an inclined spinning disk subjected to Rosseland heat and internal heat production. Mahanthesh et al.[42] used the Buongiorno model to investigate the dynamics of two-phase particulate nanofluids over a vertical plate. Naga Santoshi et al.[43] presented the numerical simulations of the 3-directional flow of Casson–Carreau nanomaterial. However, the published studies related to 3-directional flow Casson nanofluid flow using the Buongiorno model over a rotating stretchable surface are quite limited. In addition, a review paper that deals with the heating/cooling processes of suspended nanomaterials in lubricants and refrigerants are presented by Yang et al.[44].

With regards to the thermo-migration of nanoparticles in the motion of various fluids, all relevant published papers in the literature have reported the reason behind this is that the concentration decreases with thermophoresis after the formation of a relatively particle-free layer near the surface due to the migration of tiny particles through thermophoresis. The impact of thermophoresis shall be ignored when considering either the energy flux results from the composition gradient or the mass flux created by a temperature gradient. The presence of different responses to the force caused by a temperature gradient is adequate to augment the temperature distribution due to an increase in thermophoresis For Newtonian liquids, the impact of thermophoresis on the nanoparticle's concentration decreases. In contrast, the impact increases for nonNewtonian liquids. The current paper utilizes a similar model as Owhaib et al.[45], using the bvp5c algorithm and Buongiorno nanoliquids model. They mathematically studied the boundary value problem of an elongated rotating plate with constant heat flux with thermal radiation. Among the physical observation, they conclude that the nanofluid single-phase model is inadequate to study their problem.

The main objective of the current investigation is to study the 3D rotating flow of Casson liquid over an elongated flat frame exposed to a constant heat flux condition with viscous heating. The nanoparticle's haphazard movement and thermo-migration are incorporated in the model utilizing the Buongiorno model. The model is solved using the MATLAB bvp5c algorithm. The obtained results are analyzed and presented in graphs to display the impact of various parameters such as *Nb*, *Nt*, *Ec*, *Ca*, *Pr*, *Le*, and *Ro* on velocity, temperature, and concentration profiles. In addition, the heat transfer rate and the friction coefficients are to be scrutinized and presented as well.

Mathematical formulation

This study considers the laminar, steady-state, three-directional flow of an elongated non-Newtonian Casson nanofluid surface over a rotating frame. The nanoliquids surface is exposed to a constant surface heat flux condition at the boundary. The Cartesian coordinate framework is aligned with *xy*-plane and the fluid region is considered at $z \geq 0$. The incompressible Casson nanoliquid rotates consistently about *z*-axis with an unvarying rate ω. Figure 1 shows a schematic diagram of the problem under investigation.

Deploying Prandtl's boundary layer approach, the current problem under investigation governing equations are defined as below (note Refs.[35,46]):

$$\frac{\partial u}{\partial x}+\frac{\partial v}{\partial y}+\frac{\partial w}{\partial z}=0, \tag{1}$$

$$\rho\left(u\frac{\partial u}{\partial x}+v\frac{\partial u}{\partial y}+w\frac{\partial u}{\partial z}-2\omega v\right)=\mu\left(1+\frac{1}{Ca}\right)\frac{\partial^2 u}{\partial z^2}, \tag{2}$$

$$\rho\left(u\frac{\partial v}{\partial x}+v\frac{\partial v}{\partial y}+w\frac{\partial v}{\partial z}+2\omega u\right)=\mu\left(1+\frac{1}{Ca}\right)\frac{\partial^2 v}{\partial z^2}, \tag{3}$$

$$\begin{aligned}\rho C_p\left(u\frac{\partial T}{\partial x}+v\frac{\partial T}{\partial y}+w\frac{\partial T}{\partial z}\right)=k\frac{\partial^2 T}{\partial z^2}+\left(\rho C_p\right)_{np}\left\{D_B\frac{\partial T}{\partial z}\frac{\partial C}{\partial z}+\frac{D_T}{T_\infty}\left(\frac{\partial T}{\partial z}\right)^2\right\}\\ +\mu\left(1+\frac{1}{Ca}\right)\left(\left(\frac{\partial u}{\partial z}\right)^2+\left(\frac{\partial v}{\partial z}\right)^2\right)\end{aligned}, \tag{4}$$

$$u\frac{\partial C}{\partial x}+v\frac{\partial C}{\partial y}+w\frac{\partial C}{\partial z}=D_B\frac{\partial^2 C}{\partial z^2}+\frac{D_T}{T_\infty}\frac{\partial^2 T}{\partial z^2}, \tag{5}$$

where Ca-dimensionless Casson fluid factor, u, v, and w are velocities along x, y and z-directions, $\nu=\frac{\mu}{\rho}$ is the kinematic viscosity, μ is the dynamic viscosity, ρ is the density, T is the temperature, C is the nanoparticle concentration, $\alpha=\frac{k}{\rho C_p}$ is the thermal diffusivity, k is the thermal conductivity, ρC_p is the specific heat of the Casson fluid, $\left(\rho C_p\right)_{np}$ is the specific heat of the nanoparticles, D_B is the coefficient of Brownian diffusion, D_T is the coefficient of thermo-migration diffusion and T_∞ is the ambient temperature.

The pertinent boundary conditions are

$$\left.\begin{aligned}&w=v=0,\ u=U_w=ax,\ -k\left(\tfrac{\partial T}{\partial z}\right)=q_w,\ C=C_w\ at\ z=0,\\ &v=0,\ u=0,\ T=T_\infty,\ C=C_\infty\ as\ z\to\infty\end{aligned}\right\}, \tag{6}$$

where a is stretching rate and $q_w=(T_w-T_\infty)k\sqrt{a/\nu}$ is constant heat flux.

Upon considering

$$\zeta=z\sqrt{\frac{u_w}{xv}}, u=axf'(\zeta), v=axg(\zeta), w=-\sqrt{\nu a}f(\zeta),$$

$$T=(T_w-T_\infty)\theta(\zeta)+T_\infty, C=(C_w-C_\infty)\Theta(\zeta)+C_\infty. \tag{7}$$

Equation (1) is satisfied and the other Eqs. (2)–(6) yield

$$\left(1+\frac{1}{Ca}\right)f'''+ff''-f'^2+2Rog=0, \tag{8}$$

$$\left(1+\frac{1}{Ca}\right)g''+fg'-gf'-2Rof'=0, \tag{9}$$

$$\frac{1}{Pr}\theta''+f\theta'+Nb\Theta'\theta'+Nt\Theta'^2+Ec\left(1+\frac{1}{Ca}\right)\left(\left(f''\right)^2+\left(g'\right)^2\right)=0, \tag{10}$$

$$\Theta''+\frac{Nt}{Nb}\theta''+Lef\Theta'=0, \tag{11}$$

$$\left.\begin{aligned}&f=0,g=0,f'=1,\theta'=-1,\Theta=1\ at\ \zeta=0\\ &f'=0,f=0,\theta=0,\Theta=0\ as\ \zeta\to\infty.\end{aligned}\right\}, \tag{12}$$

where ζ—similarity variable, $f, g,\ \theta$, and Θ are dimensionless axial velocity, transverse velocity, temperature, and nanoparticle concentration correspondingly, $Pr=\frac{C_p\mu}{k}$(Prandtl number), $Ro=\frac{\omega}{a}$ (rotation parameter), $Le=\frac{\nu}{D_B}$(Lewis number), $Nt=\frac{\left(\rho C_p\right)_{np}D_T(T_w-T_\infty)}{\rho C_{p_2}T_\infty\nu}$ (thermophoresis parameter), $Nb=\frac{\left(\rho C_p\right)_{np}D_B(C_w-C_\infty)}{\rho C_p\nu}$ (Brownian motion parameter), and $Ec=\frac{u_w^2}{C_{p_1}(T_w-T_\infty)}$ (Eckert number).

The dimensionless expressions of friction factors, Nusselt number, and Sherwood number are given below;

$$Re_x^{0.5} Sf_x = \left(1 + \frac{1}{Ca}\right) f''(0),$$

$$Re_y^{0.5} Sf_y = \left(1 + \frac{1}{Ca}\right) g''(0),$$

$$Re_x^{-0.5} Nu_x = -\frac{1}{\theta(0)},$$

$$Re_x^{-0.5} Sh_x = -\Theta'(0), \tag{13}$$

where $Re_x = \frac{u_w(x)x}{\nu_l}$ is Reynolds number.

Numerical technique

The nonlinear boundary value problem defined in Eqs. (8)–(12) is solved numerically utilizing the bvp5c routine by letting $f = y_1, f' = y_2, f'' = y_3, g = y_4, g' = y_5, \theta = y_6, \theta' = y_7, \Theta = y_8$ and $\Theta' = y_9$ to obtain the following single-order differential system:

$$y_1' = y_2, \tag{14}$$

$$y_2' = y_3, \tag{15}$$

$$y_3' = \left(\frac{Ca}{1+Ca}\right)\left(y_2^2 - y_1 y_3 - 2Roy_4\right), \tag{16}$$

$$y_4' = y_5, \tag{17}$$

$$y_5' = \left(\frac{Ca}{1+Ca}\right)\left(2Roy_2 + y_2 y_4 - y_1 y_5\right), \tag{18}$$

$$y_6' = y_7, \tag{19}$$

$$y_7' = -\Pr\left\{ \begin{array}{l} y_1 y_7 + Nby_7 y_9 + Nt\left(y_7\right)^2 + \\ \left(1 + \frac{1}{Ca}\right) Ec\left(y_3^2 + y_5^2\right) \end{array} \right\}, \tag{20}$$

$$y_8' = y_9, \tag{21}$$

$$y_9' = -Ley_1 y_9 + \left(\frac{Nt}{Nb}\right)\Pr\left\{ \begin{array}{l} y_1 y_7 + Nby_7 y_9 + Nt\left(y_7\right)^2 + \\ \left(1 + \frac{1}{Ca}\right) Ec\left(y_3^2 + y_5^2\right) \end{array} \right\}, \tag{22}$$

with

$$y_1(0) = 0, y_4(0) = 0, y_2(0) = 1, y_8(0) = 1, y_7(0) = -1,$$

$$y_2(\infty) = 0, y_4(\infty) = 0, y_6(\infty) = 0, y_8(\infty) = 0. \tag{23}$$

The system first-order governing equations are solved using the MATLAB—bvp5c routine (see Ref.[47]). This routine integrates a system of differential equations of the form y′ = f(x,y), subject to the boundary conditions. It is using the finite difference method with achievable accuracy of 10^{-8}. Condition at infinity is rescaled to 5. For method validation, the obtained numeric solution $-\theta'(0)$ is compared with the published studies at $Nb = Nt = \lambda = \beta_E = \phi = 0$ and $Bi = 10{,}000$. Table 1 data reveals that the current study results are in good agreement with the data in the literature. In the next section, a parametric analysis is performed.

Interpretation of the outcomes

The Casson nanoliquid 3D rotating flow over a linearly stretched surface in the presence of viscous heating, Brownian movement, thermo-migration, and heat flux condition is studied. The study numeric solution presented in Figs. 2, 3, 4, 5, 6, 7, 8, 9, 10, 11, 12, 13, 14, 15, 16, 17, 18, 19, 20, 21, 22, 23, 24, 25, 26 and 27 show the parametric analysis of the prime parameters such as rotation parameter (Ro), Casson fluid factor (Ca), thermo-migration parameter (Nt), Eckert number (Ec), Lewis number (Le), Brownian movement factor (Nb) and Prandtl factor (Pr) on velocities ($f'(\eta), g(\eta)$), temperature ($\theta(\eta)$), nanoparticle concentration ($\Theta(\eta)$), friction coefficients at the plate ($Re_x^{0.5} Sf_x$ & $Re_y^{0.5} Sf_y$), Sherwood number ($Re_x^{-0.5} Sh_x$) and ($Re_x^{-0.5} Nu_x$) Nusselt number distributions.

Pr_1	Khan and Pop[38]	Gorla and Sidawi[46]	Present (bvp5c)
0.07	0.0663	0.0656	0.06562
0.2	0.1691	0.1691	0.16909
0.7	0.4539	0.5349	0.45392
2	0.9113	0.9114	0.91136
7	1.8954	1.8905	1.89542

Table 1. Comparison of $-\theta'(0)$ values with of Khan and Pop[38] and Gorla and Sidawi[46] when $Nb = Nt = \lambda = \beta_E = \phi = 0$ and $Bi = 10{,}000$.

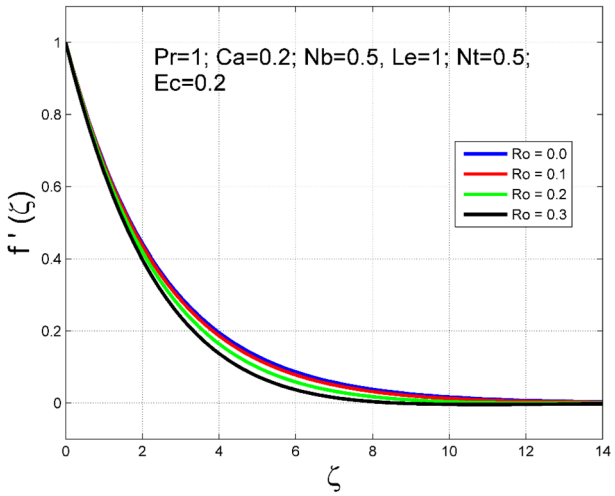

Figure 2. Effect of Ro on $f'(\zeta)$.

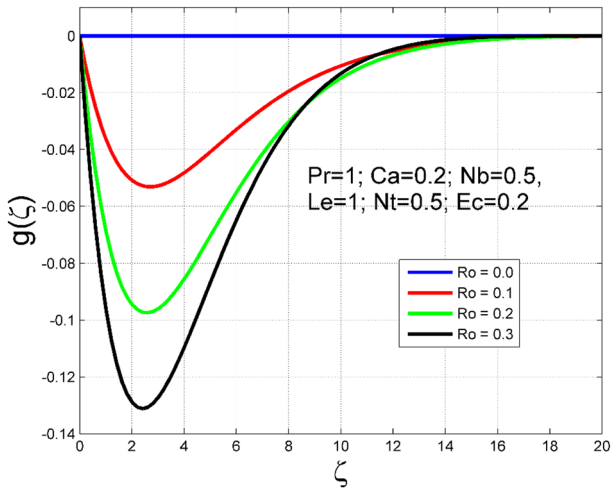

Figure 3. Effect of Ro on $g(\zeta)$.

Figures 2, 3, 4, 5, 6, 7, 8, 9, 10, 11, 12, 13, 14, 15, 16, 17, 18, 19, 20, 21, 22, 23, 24, 25, 26 and 27 are plotted for $Pr = 1, Ro = 0.5, Nb = Nt = 0.5, Le = 1, Ca = 0.2, Ec = 0.2$, and $\zeta_\infty = 20$.

The influence of rotation aspect (Ro) on velocities $(f'(\zeta), g(\zeta))$, temperature $(\theta(\zeta))$, and nanoparticle concentration $(\Theta(\zeta))$ is accessible in Figs. 2, 3, 4 and 5 correspondingly. The ratio of angular velocity rate and elongating velocity rate is termed as a rotation factor. Higher values of rotation factor designate to lesser elongating velocity rate, as a result, the magnitude of velocities are reduced by increasing values of Ro. Figures 4 and 5 show that temperature $\theta(\eta)$ and nanoparticle concentration $(\Theta(\eta))$ increased with increasing rotation factor (Ro). In

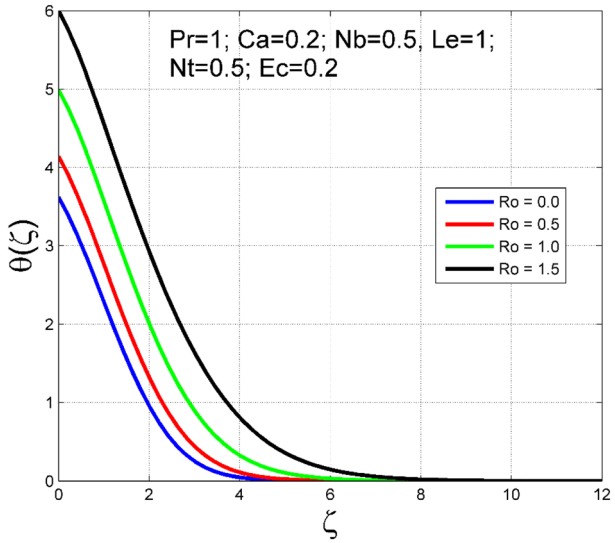

Figure 4. Effect of Ro on $\theta(\zeta)$.

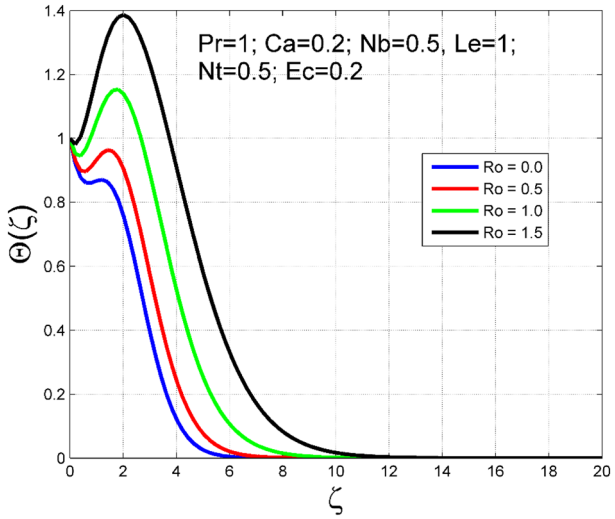

Figure 5. Effect of Ro on $\Theta(\zeta)$.

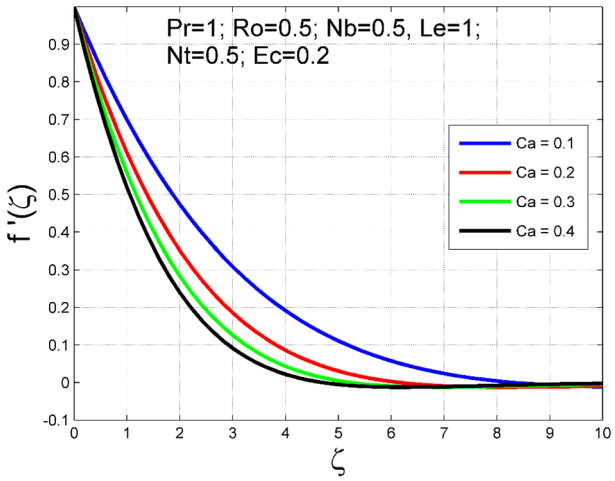

Figure 6. Effect of Ca on $f'(\zeta)$.

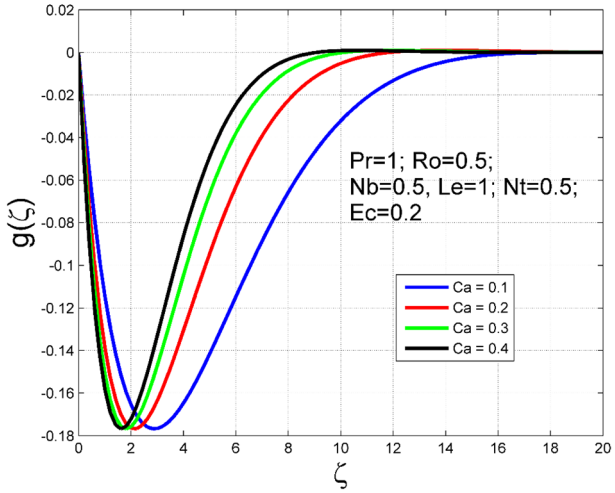

Figure 7. Effect of Ca on $g(\zeta)$.

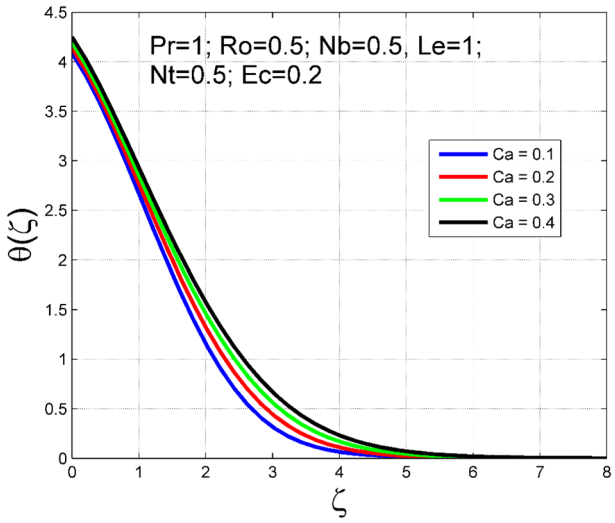

Figure 8. Effect of Ca on $\theta(\zeta)$.

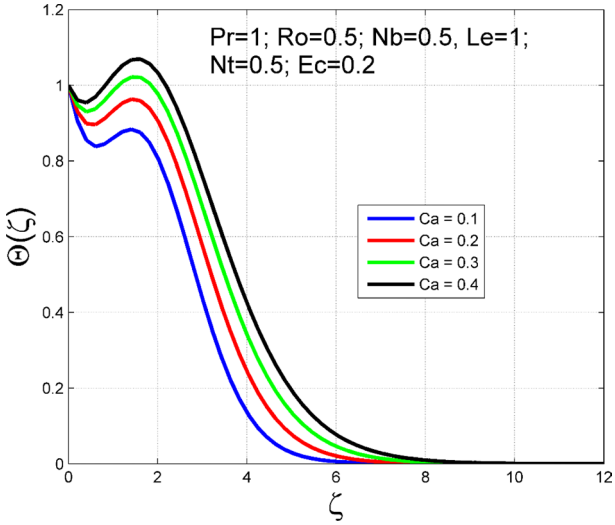

Figure 9. Effect of Ca on $\Theta(\zeta)$.

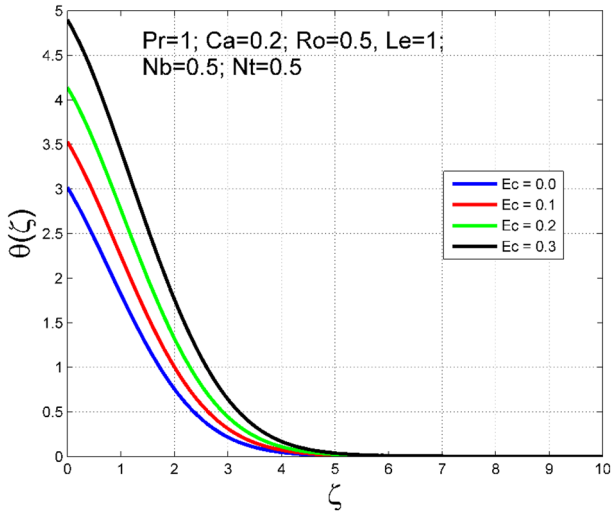

Figure 10. Effect of *Ec* on $\theta(\zeta)$.

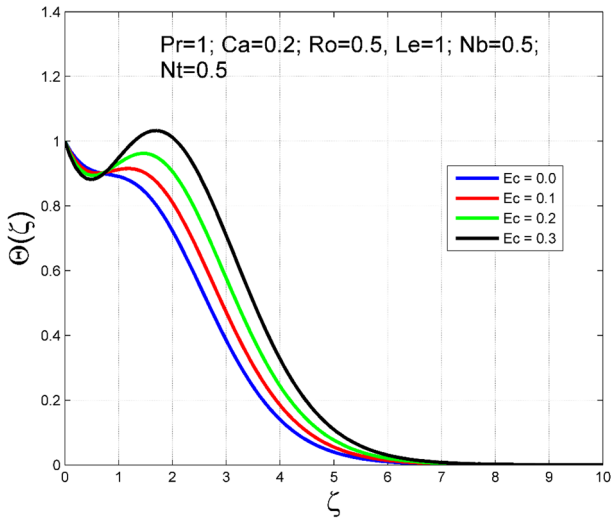

Figure 11. Effect of *Ec* on $\Theta(\zeta)$.

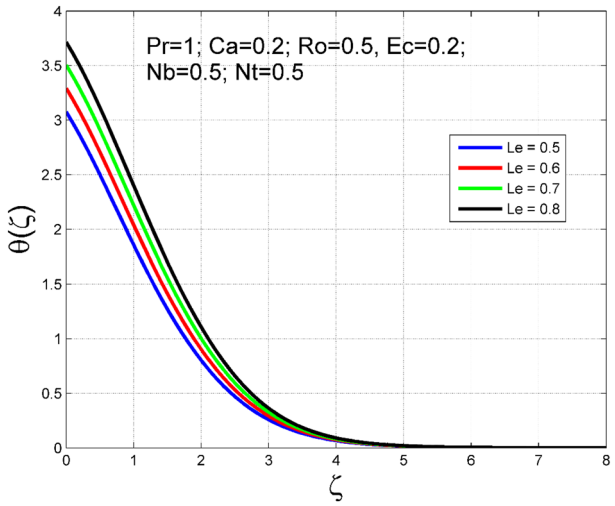

Figure 12. Effect of *Le* on $\theta(\zeta)$.

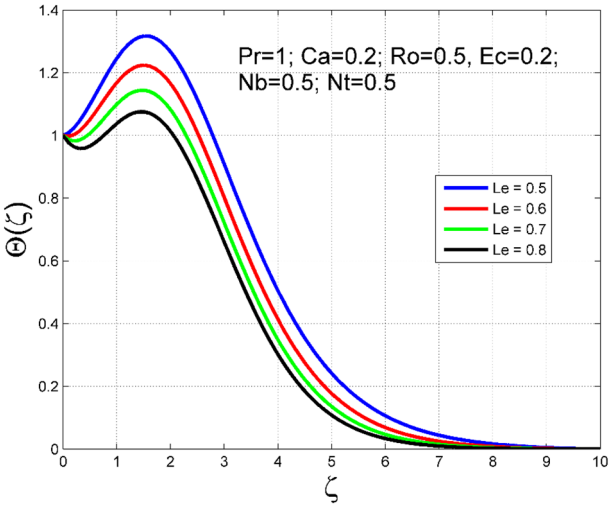

Figure 13. Effect of Le on $\Theta(\zeta)$.

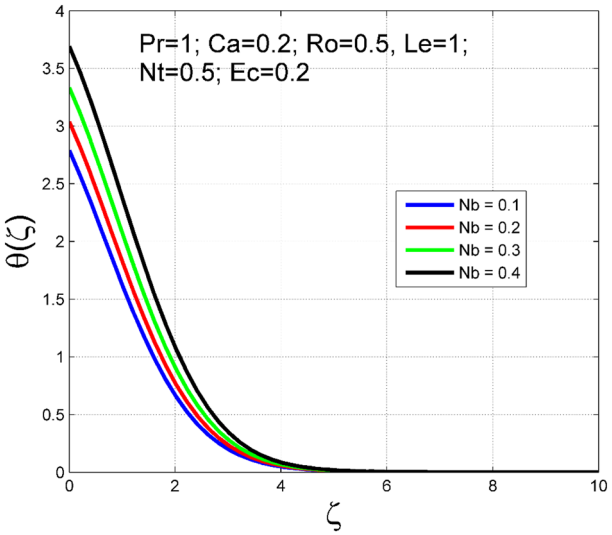

Figure 14. Effect of Nb on $\theta(\zeta)$.

addition, there is no transverse velocity in the absence of rotation factor ($Ro = 0$) and the axial velocity layer thickness was found to be higher. In contrast, the thermal and nanoparticle concentration layer structure is suppressed in the absence of rotation factor ($Ro = 0$). Figures 6, 7, 8 and 9 designate how the Casson fluid factor (Ca) disturbs the velocities ($f'(\zeta), g(\zeta)$), temperature ($\theta(\zeta)$), and nanoparticle concentration ($\Theta(\zeta)$) fields. A decreasing tendency is detected for the axial velocity layer structure when Ca values are increased (see Fig. 6), while this trend is opposite for the thermal and nanoparticles concentration layer structure (see Figs. 8, 9). In Fig. 7, the magnitude of the transverse velocity ($g(\zeta)$) decreases near the elongated plate, and then it increases for larger values of Ca.

The importance of Eckert number (Ec) on temperature ($\theta(\zeta)$) and nanoparticle concentration ($\Theta(\zeta)$) distributions are outlined in Figs. 10 and 11 correspondingly. Improving the tendency of temperature ($\theta(\zeta)$) and nanoparticle concentration ($\Theta(\zeta)$) layer structure is found for progressive values of Ec. The kinetic energy is directly related to the Eckert number (Ec). As Ec increases, the kinetic energy strength increases, consequently, the magnitude of temperature ($\theta(\zeta)$) and nanoparticle concentration ($\Theta(\zeta)$) enhances for higher values of Ec. The consequence of Le on temperature ($\theta(\zeta)$) and nanoparticle concentration ($\Theta(\zeta)$) distributions are delineated in Figs. 12 and 13. By definition, higher Le corresponds to stronger thermal diffusivity and lower mass diffusivity. Stronger thermal diffusivity is accountable for thicker thermal layer structure (see Fig. 12), similarly, a lower mass diffusivity is accountable for thinner nanoparticle concentration layer structure (see Fig. 13).

To analyze the effects of nanoparticles on the dynamics of Casson fluid through Brownian movement (Nb) and thermo-diffusion of nanoparticles (Nt), Figs. 14, 15, 16 and 17 are presented. The arbitrary movement of nanoparticles generates supplementary internal heat in the Casson fluid due to collision, and this is accountable

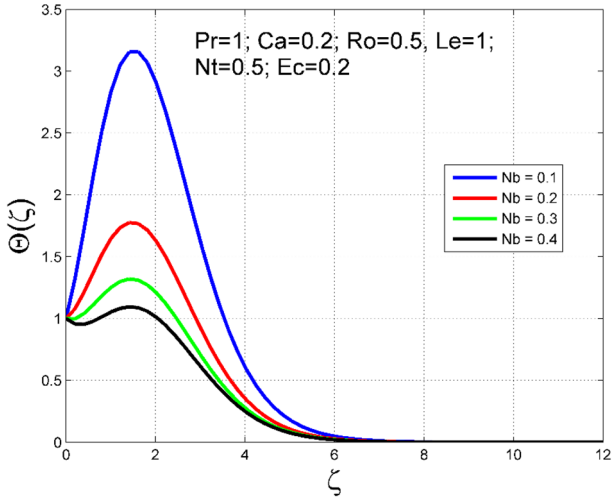

Figure 15. Effect of *Nb* on $\Theta(\zeta)$.

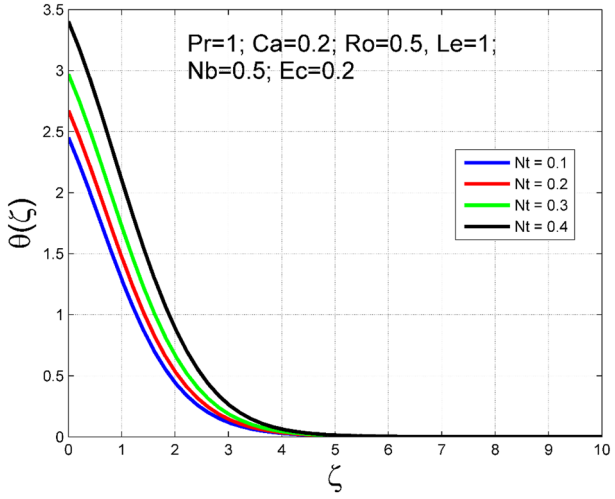

Figure 16. Effect of *Nt* on $\theta(\zeta)$.

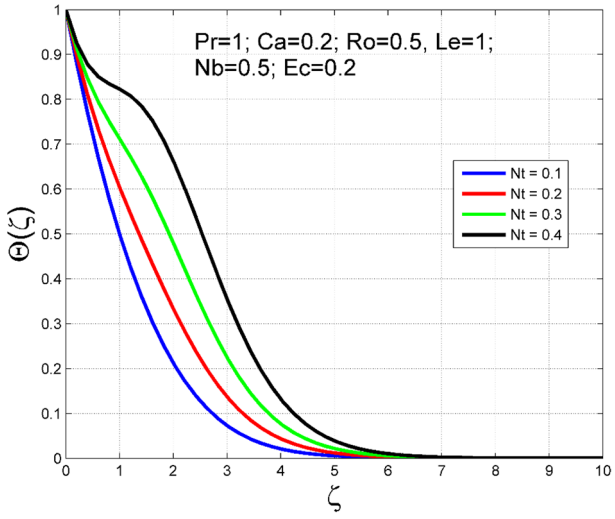

Figure 17. Effect of *Nt* on $\Theta(\zeta)$.

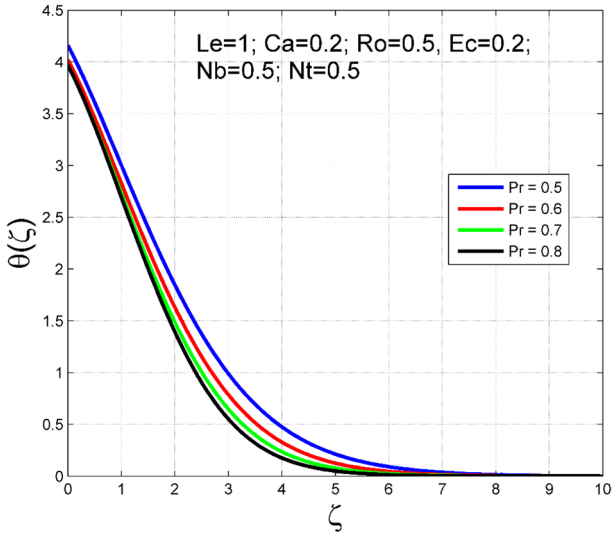

Figure 18. Effect of Pr on $\theta(\zeta)$.

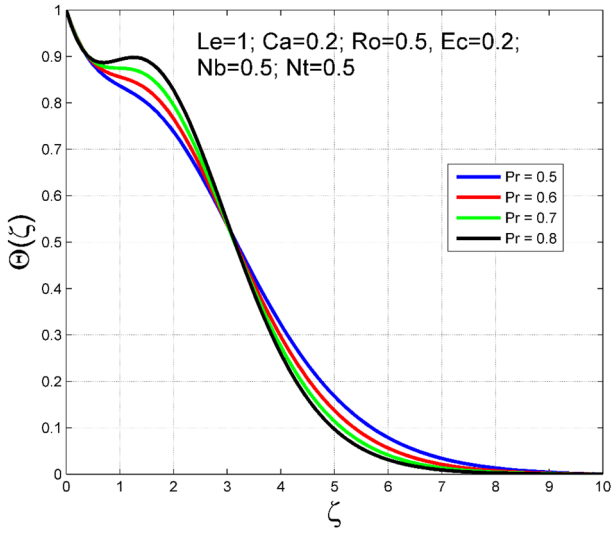

Figure 19. Effect of Pr on $\Theta(\zeta)$.

for improvement in the thermal field (see Fig. 14). In Fig. 15, the nanoparticle concentration field diminished significantly for enlarging values of Nb. On the other hand. The thermophoresis mechanism is related to thermal gradient and that produces additional heat in the Casson fluid system and thereby the magnitude of temperature and nanoparticles concentration fields increased (see Figs. 16, 17). Thus one can conclude that the thermal layer structure of Casson fluid improved notably by conveying nanoparticles. Figures 18 and 19 display the influence of Prandtl number (Pr) on temperature ($\theta(\zeta)$) and nanoparticle concentration ($\Theta(\zeta)$). A significant decrement occurred in $\theta(\zeta)$ via higher Pr. Higher Pr corresponds to the lower thermal conductivity of the Casson fluid, which causes a decrement in the magnitude of the temperature field (see Fig. 18). In Fig. 19, the nanoparticle concentration ($\Theta(\zeta)$) increases near the plate and decreases far away from the plate by increasing numeric values of Pr.

Figures 20 and 21 visualize the impact of rotation factor (Ro) and Casson fluid factor (Ca) on the plate friction factors along x and y directions ($Re_x^{0.5}Sf_x, Re_y^{0.5}Sf_y$) respectively when $Nb = Nt = 0.5, Le = 1, Pr = 1, Ec = 0.2$ and $\zeta_\infty = 20$. Here both $Re_x^{0.5}Sf_x$ and $Re_y^{0.5}Sf_y$ are upsurged for increasing values of Ro. This is because the velocities layer structure is thinner at the plate for larger values of Ro. While the $Re_x^{0.5}Sf_x$ and $Re_y^{0.5}Sf_y$ are diminished for cumulative values of Ca (see Fig. 21). Figures 22 and 23 are drawn to examine the stimulus of Nb and Nt on $\mathrm{Re}_x^{-0.5}Nu_x$ and $Re_x^{-0.5}Sh_x$ correspondingly. Here the heat transfer rate at the plate $\mathrm{Re}_x^{-0.5}Nu_x$ is found maximum when both Nb and Nt values are set higher (see Fig. 22). Whereas, the enhancing and declining tendency of $Re_x^{-0.5}Sh_x$ is seen for larger values of Nt and Nb respectively (see Fig. 23). Figures 24 and 25 depict the influences of Ec and Ca on $\mathrm{Re}_x^{-0.5}Nu_x$ and $Re_x^{-0.5}Sh_x$ correspondingly. Figure 24 exhibits that $\mathrm{Re}_x^{-0.5}Nu_x$ increases for larger

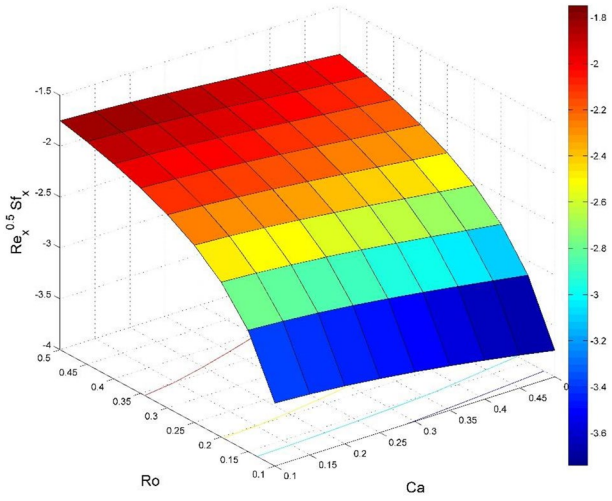

Figure 20. Effect of *Ca* and *Ro* on $\mathrm{Re}_x^{0.5} Sf_x$.

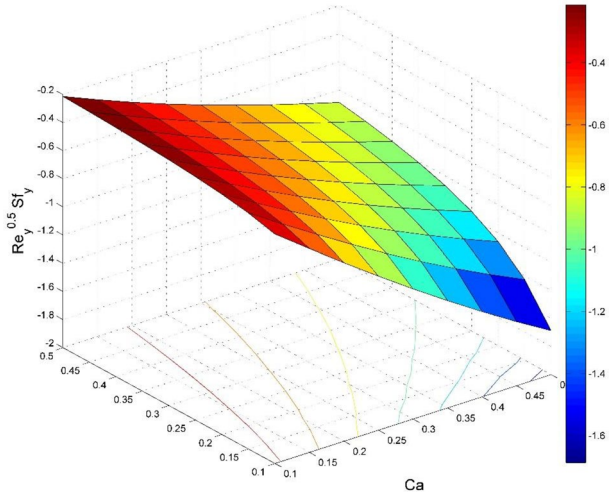

Figure 21. Effect of *Ca* and *Ro* on $\mathrm{Re}_y^{0.5} Sf_y$.

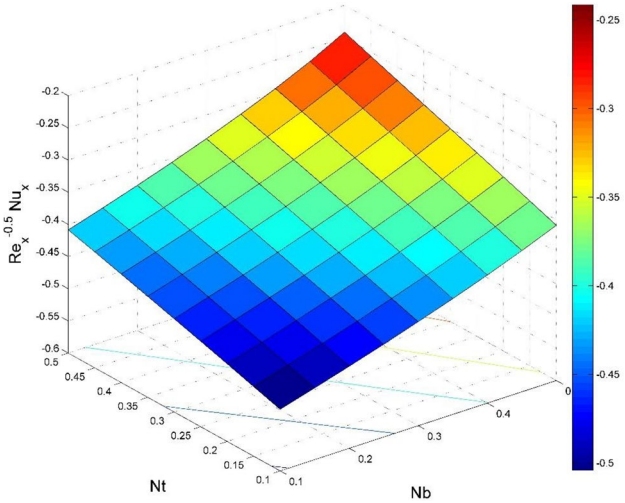

Figure 22. Effect of *Nb* and *Nt* on $\mathrm{Re}_x^{-0.5} Nu_x$.

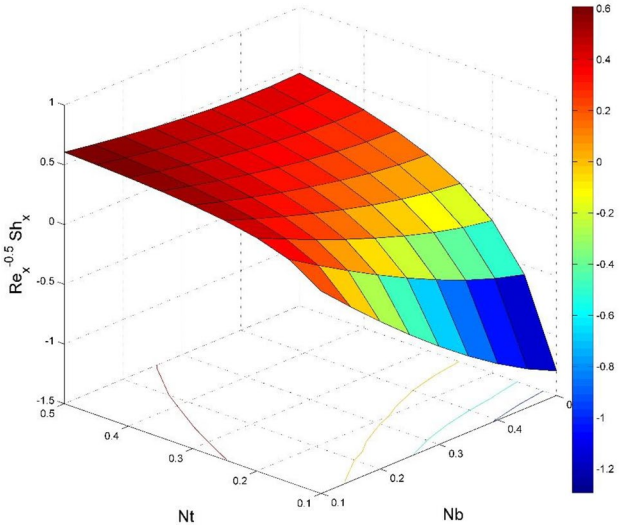

Figure 23. Effect of *Nb* and *Nt* on $\mathrm{Re}_x^{-0.5} Sh_x$.

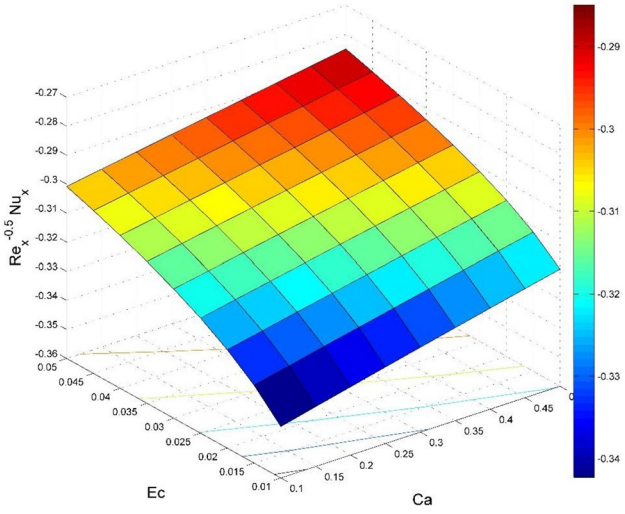

Figure 24. Effect of *Ec* and *Ca* on $\mathrm{Re}_x^{-0.5} Nu_x$.

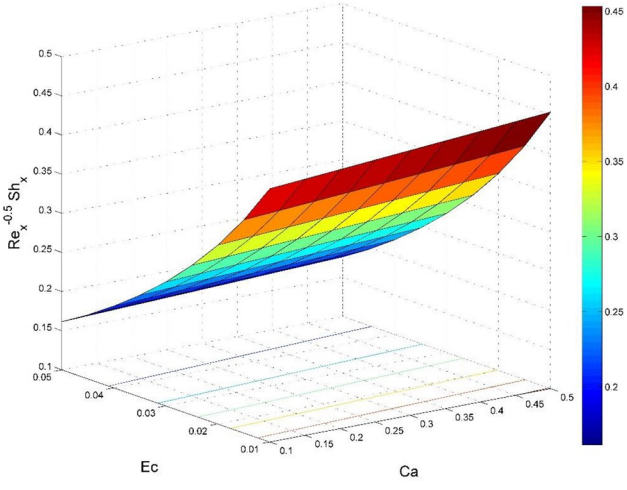

Figure 25. Effect of *Ec* and *Ca* on $\mathrm{Re}_y^{-0.5} Sh_x$.

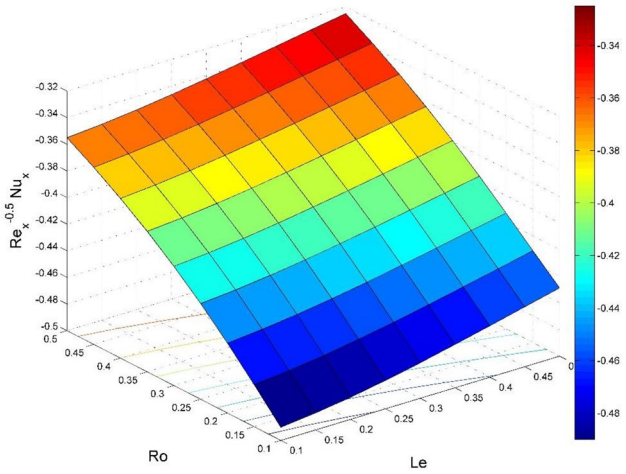

Figure 26. Effect of *Ro* and *Le* on $\mathrm{Re}_{\mathrm{x}}^{-0.5} Nu_x$.

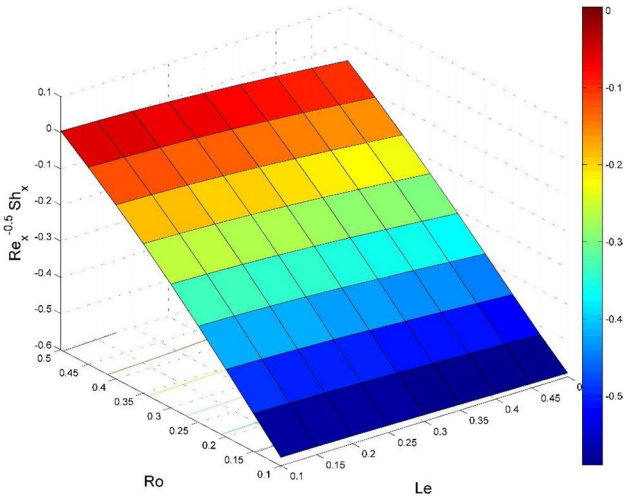

Figure 27. Effect of *Ro* and *Le* on $\mathrm{Re}_{\mathrm{y}}^{-0.5} Sh_x$.

Ec and *Ca*. In Fig. 25, the mass transfer rate at the plate $Re_x^{-0.5} Sh_x$ is found maximum when *Ec* is kept lower value and the value of *Ca* set to higher. Figures 26 and 27 elucidate the performance of $\mathrm{Re}_{\mathrm{x}}^{-0.5} Nu_x$ and $Re_x^{-0.5} Sh_x$ for distinct values of *Ro* and *Le*. Figure 26 exhibits that the $\mathrm{Re}_{\mathrm{x}}^{-0.5} Nu_x$ increases for larger *Ro* and *Le*. However, the $Re_x^{-0.5} Sh_x$ is an increasing property of *Ro* and decreasing property of *Le*.

Final remarks. The major findings of the current research work are given below:

- An elevation in the strength of Coriolis force exhibits similar behavior for both axial and transverse velocities.
- Stronger Coriolis force exerted by rotation improves the thermal layer structure.
- The nanoparticle concentration is found higher due to the rotation aspect and Casson fluid parameter.
- The viscous dissipation effect leads to an enhancement of nanoparticle concentration and temperature profiles.
- There is no transverse velocity in the absence of rotation factor while the axial velocity layer thickness was found to be higher in the absence of rotation factor.
- The Casson fluid factor exhibits decreasing behavior of velocities, while the opposite trend is observed for the larger Casson fluid factor.
- The thermo-diffusion due to nanoparticles is accountable for thermal and solute layer thickness growth.
- Temperature layer thickness enlarges owing to the nanoparticles' random movement.
- Temperature and nanoparticle's concentration layer thickness improves for larger Eckert number.
- The friction factor increased for the larger rotation factor.
- The heat transfer rate at the plate is found maximum when both *Nb* and *Nt* values are set higher.

Received: 3 July 2021; Accepted: 4 March 2022
Published online: 11 March 2022

References

1. Andersson, H. I. & Dandapat, B. S. Flow of a power law fluid over a stretching sheet. *Appl. Anal. Contin. Media* **1**, 339–347 (1991).
2. Hassanien, I. A. Flow and heat transfer on a continuous flat surface moving in a parallel free stream of power-law fluid. *Appl. Model* **20**(10), 779–784 (1996).
3. Sadeghy, K. & Sharifi, M. Local similarity solution for the flow of a 'second-grade' viscoelastic fluid above a moving plate. *Int. J. Non-linear Mech.* **39**, 1265–1273 (2004).
4. Serdar, B. & Salih Dokuz, M. Three-dimensional stagnation point flow of a second grade fluid towards a moving plate. *Int. J. Eng. Sci.* **44**, 49–58 (2006).
5. Sajid, M., Hayat, T. & Asgharm, S. Non-similar analytic solution for MHD flow and heat transfer in a third-order fluid over a stretching sheet. *Int. J. Heat Mass Transf.* **50**, 1723–1736 (2007).
6. Sajid, M., Ahmad, I., Hayat, T. & Ayub, M. Unsteady flow and heat transfer of a second grade fluid over a stretching sheet. *Commun. Nonlinear Sci. Numer. Simul.* **14**, 96–108 (2009).
7. Aksoy, Y., Pakdemirli, M. & Khalique, C. M. Boundary layer equations and stretching sheet solutions for the modified second grade fluid. *Int. J. Eng. Sci.* **45**, 829–841 (2007).
8. Hayat, T., Awais, M. & Sajid, M. Mass transfer effects on the unsteady flow of UCM fluid over a stretching sheet. *Int. J. Mod. Phys. B* **25**, 2863–2878 (2011).
9. Fung, Y. C. *Biodynamics Circulation* (Springer, 1984).
10. Dash, R. K., Mehta, K. N. & Jayaraman, G. Casson fluid flow in a pipe filled with a homogeneous porous medium. *Int. J. Eng. Sci.* **34**(10), 1145–1156 (1996).
11. Pramanik, S. Casson fluid flow and heat transfer past an exponentially porous stretching surface in presence of thermal radiation. *Ain Shams Eng. J.* **5**(1), 205–212 (2014).
12. Shaw, S., Mahanta, G. & Sibanda, P. Non-linear thermal convection in a Casson fluid flow over a horizontal plate with convective boundary condition. *Alex. Eng. J.* **55**(2), 1295–1304 (2016).
13. Tamoor, M., Waqas, M., Khan, M. I., Alsaedi, A. & Hayat, T. Magnetohydrodynamic flow of Casson fluid over a stretching cylinder. *Results Phys.* **7**, 498–502 (2017).
14. Animasaun, I. L. Effects of thermophoresis, variable viscosity and thermal conductivity on free convective heat and mass transfer of non-darcian MHD dissipative Casson fluid flow with suction and nth order of chemical reaction. *J. Niger. Math. Soc.* **34**(1), 11–31 (2015).
15. Raju, C. S. K. & Sandeep, N. Unsteady three-dimensional flow of Casson-Carreau fluids past a stretching surface. *Alex. Eng. J.* **55**(2), 1115–1126 (2016).
16. Nadeem, S., Haq, R. U., Akbar, N. S. & Khan, Z. H. MHD Casson fluid flow past a porous linearly stretching sheet. *Alex. Eng. J.* **52**(4), 577–582 (2013).
17. Shehzad, S. A., Hayat, T. & Alsaedi, A. Three-dimensional MHD flow of Casson fluid in porous medium with heat generation. *J. Appl. Fluid Mech.* **9**(1), 215–223 (2016).
18. Zia, Q. Z., Ullah, I., Waqas, M. A., Alsaedi, A. & Hayat, T. Cross diffusion and exponential space dependent heat source impacts in radiated three-dimensional (3D) flow of Casson fluid by heated surface. *Results Phys.* **8**, 1275–1282 (2018).
19. Prasad, P. D., Saleem, S., Varma, S. V. K. & Raju, C. S. K. Three dimensional slip flow of a chemically reacting Casson fluid flowing over a porous slender sheet with a non-uniform heat source or sink. *J. Korean Phys. Soc.* **74**(9), 855–864 (2019).
20. Salahuddin, T., Arshad, M., Siddique, N., Alqahtani, A. S. & Malik, M. Y. Thermophysical properties and internal energy change in Casson fluid flow along with activation energy. *Ain Shams Eng. J.* **11**(4), 1355–1365 (2020).
21. Choi, S. U. S. & Eastman, J. A. Enhancing thermal conductivity of fluids with nanoparticles. In *Proc. ASME Int. Mech. Eng. Congress & Exposition*, Vol. 66 (1995).
22. Rashidi, M. M., Sadri, M. & Sheremet, M. A. Numerical simulation of hybrid nanofluid mixed convection in a lid-driven square cavity with magnetic field using high-order compact scheme. *Nanomaterials* **11**(9), 2250 (2021).
23. Rashidi, M. M., Ghahremanian, S., Toghraie, D. & Roy, P. Effect of solid surface structure on the condensation flow of argon in rough nanochannels with different roughness geometries using molecular dynamics simulation. *Int. Commun. Heat Mass Transf.* **117**, 104741 (2020).
24. Bhatti, M. M., Mishra, S. R., Abbas, T. & Rashidi, M. M. A mathematical model of MHD nanofluid flow having gyrotactic microorganisms with thermal radiation and chemical reaction effects. *Neural Comput. Appl.* **30**, 1237–1249 (2018).
25. Al-Kouz, W. G., Kiwan, S., Alkhalidi, A., Sari, M. E. & Alshare, A. Numerical study of heat transfer enhancement for low-pressure flows in a square cavity with two fins attached to the hot wall using Al_2O_3-air nanofluid. *Strojniški Vestnik J. Mech. Eng.* **64**(1), 26–36 (2018).
26. Al-Kouz, W. *et al.* Entropy generation optimization for rarified nanofluid flows in a square cavity with two fins at the hot wall. *Entropy* **21**(2), 103 (2019).
27. Abu-Libdeh, N. *et al.* Hydrothermal and entropy investigation of Ag/MgO/H_2O hybrid nanofluid natural convection in a novel shape of porous cavity. *Appl. Sci.* **11**(4), 1722 (2021).
28. Mahanthesh, B., Mackolil, J., Radhika, M. & Al-Kouz, W. Significance of quadratic thermal radiation and quadratic convection on boundary layer two-phase flow of a dusty nanoliquid past a vertical plate. *Int. Commun. Heat Mass Transf.* **120**, 105029 (2021).
29. Mukhtar, T., Jamshed, W., Aziz, A. & Al-Kouz, W. Computational investigation of heat transfer in a flow subjected to magnetohydrodynamic of Maxwell nanofluid over a stretched flat sheet with thermal radiation. *Num. Method Part. Diff. Eq.* https://doi.org/10.1002/num.22643 (2020).
30. Alshare, A., Al-Kouz, W., Alkhalidi, A., Kiwan, S. & Chamkha, A. Periodically fully developed nanofluid transport through a wavy module. *J. Therm. Anal. Calorim.* **144**(3), 779–791 (2021).
31. Al-Kouz, W., Al-Waked, R., Sari, M. E., Owhaib, W. & Atieh, A. Numerical study of heat transfer enhancement in the entrance region for low-pressure gaseous laminar pipe flows using Al_2O_3–air nanofluid. *Adv. Mech. Eng.* **10**(7), 1687814018784410 (2018).
32. Waqas, H., Imran, M., Muhammad, T., Sait, S. M. & Ellahi, R. On bio-convection thermal radiation in Darcy-Forchheimer flow of nanofluid with gyrotactic motile microorganism under Wu's slip over stretching cylinder/plate. *Int. J. Numer. Methods Heat Fluid Flow* **31**(5), 1520–1546 (2021).
33. Zhang, L. *et al.* Nonlinear nanofluid fluid flow under the consequences of Lorentz forces and Arrhenius kinetics through a permeable surface: A robust spectral approach. *J. Taiwan Inst. Chem. Eng.* **124**, 98–105 (2021).
34. Tripathi, D., Prakash, J., Tiwari, A. K. & Ellahi, R. Thermal, microrotation, electromagnetic field and nanoparticle shape effects on Cu-CuO/blood flow in microvascular vessels. *Microvasc. Res.* **132**, 104065 (2020).
35. Buongiorno, J. Convective transport in nanofluids. *ASME J. Heat Transf.* **128**(3), 240–250 (2006).
36. Kuznetsov, A. V. & Nield, D. A. Natural convective boundary-layer flow of a nanofluid past a vertical plate. *Int. J. Therm. Sci.* **49**(2), 243–247 (2010).
37. Nield, D. A. & Kuznetsov, A. V. The Cheng-Minkowycz problem for natural convective boundary-layer flow in a porous medium saturated by a nanofluid. *Int. J. Heat Mass Transf.* **52**(25–26), 5792–5795 (2009).

38. Khan, W. A. & Pop, I. Boundary-layer flow of a nanofluid past a stretching sheet. *Int. J. Heat Mass Transf.* **53**(11–12), 2477–2483 (2010).
39. Gupta, S. & Sharma, K. Numerical simulation for magnetohydrodynamic three dimensional flow of Casson nanofluid with convective boundary conditions and thermal radiation. *Eng. Comput.* **34**(8), 2698–2722 (2017).
40. Nadeem, S., Haq, R. U. & Akbar, N. S. MHD three-dimensional boundary layer flow of Casson nanofluid past a linearly stretching sheet with convective boundary condition. *IEEE Trans. Nanotechnol.* **13**(1), 109–115 (2013).
41. Saeed, A. *et al.* Three-dimensional casson nanofluid thin film flow over an inclined rotating disk with the impact of heat generation/consumption and thermal radiation. *Coatings* **9**(4), 248 (2019).
42. Mahanthesh, B., Mackolil, J., Radhika, M., Al-Kouz, W. & Siddabasappa,. Significance of quadratic thermal radiation and quadratic convection on boundary layer two-phase flow of a dusty nanoliquid past a vertical plate. *Int. Commun. Heat Mass Transf.* **120**, 105029 (2021).
43. Naga Santoshi, P., Ramana Reddy, G. V. & Padma, P. Numerical scrutinization of three dimensional Casson-Carreau nanofluid flow. *J. Appl. Comput. Mech.* **6**(3), 531–542 (2020).
44. Yang, L. *et al.* A review of heating/cooling processes using nanomaterials suspended in refrigerants and lubricants. *Int. J. Heat Mass Transf.* **153**, 119611 (2020).
45. Owhaib, W., Basavarajappa, M. & Al-Kouz, W. Radiation effects on 3D rotating flow of Cu-water nanoliquid with viscous heating and prescribed heat flux using modified Buongiorno model. *Sci. Rep.* **11**, 20669 (2021).
46. Gorla, R. S. R. & Sidawi, I. Free convection on a vertical stretching surface with suction and blowing. *Appl. Sci. Res.* **52**(3), 247–257 (1994).
47. Shampine, L. F. & Kierzenka, J. A BVP solver that controls residual and error. *J. Numer. Anal. Ind. Appl. Math.* **3**(1–2), 27–41 (2008).

Author contributions

This is to confirm that the two authors had worked equally on the final article. This includes the formulation, analysis, producing figures, and discussing all the results. Moreover, the two authors had contributed equally in writing the manuscript as well.

Competing interests

The authors declare no competing interests.

Additional information

Correspondence and requests for materials should be addressed to W.A.-K.

Reprints and permissions information is available at www.nature.com/reprints.

Publisher's note Springer Nature remains neutral with regard to jurisdictional claims in published maps and institutional affiliations.